Carbohydrate Polymers 95 (2013) 760–767

Contents lists available at SciVerse ScienceDirect

Carbohydrate Polymers

journal homepage: www.elsevier.com/locate/carbpol

# Hydrogel, aerogel and film of cellulose nanofibrils functionalized with silver nanoparticles

Hong Dong[a,*], James F. Snyder[a], Dat T. Tran[b], Julia L. Leadore[a]

[a] U.S. Army Research Laboratory, Macromolecular Science & Technology Branch, Aberdeen Proving Ground, MD 21005, United States
[b] U.S. Army Research Laboratory, Electrochemistry Branch, Adelphi, MD 20783, United States

ARTICLE INFO

*Article history:*
Received 20 September 2012
Received in revised form 1 March 2013
Accepted 12 March 2013
Available online 21 March 2013

*Keywords:*
Nanocellulose
Nanofibrillated cellulose
Silver nanoparticles
Hydrogel
Aerogel
Nanocellulose film

ABSTRACT

In this work, we describe hydrogels, aerogels and films of nanofibrillated cellulose (NFC) functionalized with metal nanoparticles using silver as an example. The TEMPO process used to produce NFC generates negatively charged surface carboxylate groups that provide high binding capability to transition metal species such as $Ag^+$. The gelation of NFC triggered by transition monovalent metal ions was revealed for the first time. The interaction was utilized to bind $Ag^+$ on the NFC surface and simultaneously induce formation of NFC-$Ag^+$ hydrogels, where $Ag^+$ was slowly reduced to Ag nanoparticles by hydroxyl groups on NFC without additional reducing agent. The NFC-$Ag^+$ hydrogel was initiated by strong association of carboxylate groups on NFC with $Ag^+$ and sufficient NFC surface charge reduction. The stiff hydrogel has a storage modulus leveled off at a plateau value of ~6800 Pa. Porous aerogels and flat thin films comprising a continuous matrix of NFC were decorated with Ag nanoparticles through freeze-drying or solution-casting of NFC-$Ag^+$ dispersions with low contents of $Ag^+$, respectively, followed by UV reduction. The presence of Ag species on NFC reduced coalescence of nanofibrils in the film formation as revealed from AFM phase images.



## 1. Introduction

Nanocellulose has been of increasing interest recently as a sustainable and renewable material that has the potential for low cost and high mechanical performance (Eichhorn et al., 2010; Moon, Martini, Nairn, Simonsen, & Youngblood, 2011). Cellulose nanocrystals and cellulose nanofibrils have attracted particularly intense research interest. Cellulose nanocrystals (CNC), which can be isolated from natural cellulose fibers by controlled acid hydrolysis, are being considered for reinforcement of various polymer matrices owing to their high modulus (Dong et al., 2012; Eichhorn et al., 2010). The native cellulose nanofibrils (CNF), also referred as nanofibrillated cellulose (NFC) or microfibrillated cellulose (MFC) depending on size and production process, is an attractive biocompatible nanomaterial. Relative to CNC, NFC typically has a higher aspect ratio and is considerably more ductile thereby providing a more useful template for incorporating functionalities (Pääkkö et al., 2008), and preparing porous aerogels (Aulin, Netrval, Wågberg, & Lindström, 2010; Pääkkö et al., 2008; Sehaqui, Salajkov, Zhou, & Berglund, 2010), flat nanopapers (Henriksson, Berglund, Isaksson, Lindström, & Nishino, 2008; Sehaqui, Liu, Zhou, & Berglund, 2010) and thin films (Fukuzumi, Saito, Iwata, Kumamoto, & Isogai, 2009) that have many potential applications.

Structured hydrogel and aerogel materials derived from natural polymers such as cellulose have been considered for biomedical, cosmetic, pharmaceutical, and other applications where biocompatibility and biodegradability are required (Chang, & Zhang, 2011; Garcia-Gonzalez, Alnaief, & Smirnova, 2011; Jin, Nishiyama, Wada, & Kuga, 2004). Cellulose hydrogels are typically fabricated from native cellulose via direct cellulose dissolution. Cellulose hydrogels can be prepared from a cellulose solution through physical cross-linking because cellulose has many hydroxyl groups that can easily form hydrogen bonding linked networks (Chang, & Zhang, 2011). Cellulose aerogels are typically fabricated by dissolution of cellulose followed by a solvent exchange and drying process (Garcia-Gonzalez, Alnaief, & Smirnova, 2011; Jin, Nishiyama, Wada, & Kuga, 2004). However, cellulose is very difficult to dissolve in common solvents (Chang and Zhang, 2011). Recently, cellulose nanofibrils produced using mechanical shearing or chemical treatment were used to prepare porous cellulose aerogels that show high flexibility and high toughness (Aulin, Netrval, Wågberg, & Lindström, 2010; Pääkkö et al., 2008; Sehaqui, Salajkov, et al., 2010). Cellulose aerogels have been directly prepared by freeze-drying from "as-produced" nanofibril aqueous dispersions to yield porosities as high as 99.5% (Sehaqui, Salajkov, et al., 2010). Alternatively, super-critical $CO_2$ drying methods yield finer pores, more individualized nanofibrils and thus higher surface area than freeze-drying

* Corresponding author. Tel.: +1 410 306 4398; fax: +1 410 306 0676.
*E-mail addresses:* hong.dong.ctr@mail.mil, dong.rena@gmail.com (H. Dong).

0144-8617/$ – see front matter © 2013 Elsevier Ltd. All rights reserved.
http://dx.doi.org/10.1016/j.carbpol.2013.03.041

methods (Korhonen et al., 2011). Preparation of cellulose physical hydrogels comprising TEMPO-oxidized NFC has also been recently demonstrated by addition of a strong acid to protonate the carboxylate groups on the NFC (Saito, Uematsu, Kimura, Enomae, & Isogai, 2011). A model has been developed to predict the fibril-fibril interaction potential at a given pH in a given ionic strength environment (Fall, Lindström, Sundman, Ödberg, & Wågberg, 2011).

In addition to aerogels and hydrogels, water dispersed cellulose nanofibrils may be converted to nanopaper or other thin film structures. Highly tough nanopapers of different porosities have been previously prepared by filtering water dispersed NFC followed by solvent exchange and drying. The high toughness was attributed to the intertwined nanofibrillar network structure and high mechanical nanofibril performance (Henriksson et al., 2008). Transparent flexible films have been demonstrated using dense networks of NFC. The films had extremely low coefficients of thermal expansion and showed high oxygen barrier properties (Fukuzumi et al., 2009).

Structuring NFC into these and other architectures opens new possibilities for using functionalized surfaces to meet a variety of potential applications. However, only a few reports have appeared to date on functionalization of structured NFC materials, including the application of conductive polyaniline to achieve an electrically conductive flexible aerogel (Pääkkö et al., 2008). For metal species, previous studies have primarily focused on functionalizing single cellulose nanocrystals in a solvent dispersion (Liu, Wang, Song, & Shang, 2011; Mahmoud, Male, Hrapovic, & Luong, 2009; Padalkar et al., 2010; Shin, Bae, Arey, & Exarhos, 2008) or single cellulose fibrils in a solvent dispersion (Diez et al., 2011; Ifuku, Tsuji, Morimoto, Saimoto, & Yano, 2009; Koga et al., 2010; Wu, Kuga, & Huang, 2008) with metal nanoparticles or metal nanoclusters via various approaches.

In the current study, we investigated functionalization of structured NFC in the forms of hydrogels, aerogels and thin films. Particular focus was tuned to use of surface carboxylate groups, originating from TEMPO oxidation, and the prevalent surface hydroxyl groups to allow incorporation of organic or inorganic matters for various functionalities through covalent binding or non-covalent interactions. The high binding capability of NFC to heavy metal ions due to the presence of carboxylate groups (Saito & Isogai, 2005) was utilized to incorporate $Ag^+$ on the NFC surface, where $Ag^+$ was subsequently reduced to nanoparticles. The effect of silver ions on the gelation of the NFC aqueous dispersion was described, and the dynamic visoelastic properties of the robust gels were studied. Porous aerogels and flat thin films were also fabricated comprising continuous matrices of NFC decorated with Ag nanoparticles, and the influence of Ag species on the morphologies of these materials was investigated.

## 2. Experimental

### 2.1. Materials

An aqueous dispersion of NFC was provided courtesy of the USDA Forest Products Laboratory (Madison, Wisconsin), which was produced from wood pulp using the TEMPO oxidation technique with sodium hypochlorite as the terminal oxidant according to the method described in the literature (Saito, Kimura, Nishiyama, & Isogai, 2007). The dispersion had a concentration of 1.27 wt% NFC and a carboxylate content of 1.3 mmol per gram of dried NFC. The nanofibrils were measured from the TEM images to be 5 nm in average diameter and several hundreds of nanometers up to a micron in length (representative image shown in Fig. 1S-supplementary information). Silver nitrate ($AgNO_3$) as a precursor of silver nanoparticles was obtained from Sigma–Aldrich.

### 2.2. Preparation of NFC-Ag hydrogels and NFC hydrogels

NFC-Ag hydrogels were generated by addition of $AgNO_3$ aqueous solution to an NFC aqueous dispersion followed by spontaneous reduction. An excess amount of $AgNO_3$ was used in order to ensure complete saturation of available carboxylate groups with silver ions. Typically, the NFC dispersion was put into a crystal dish or a vial. An equal volume of 50 mM $AgNO_3$ solution was added dropwise along the sidewall into the NFC dispersion without stirring. Gelation occurred rapidly upon the addition of $AgNO_3$. The gel sat for five days to allow for slow reduction of $Ag^+$ to Ag nanoparticles. A brown gel thus formed was removed from the $AgNO_3$ solution, and immersed into water several times to rinse off the unattached Ag species.

NFC hydrogels used in the UV–vis spectroscopic study were prepared via protonation of NFC carboxylate groups. HCl (1 M) was added as a gelling agent to the NFC dispersion and the solution sat for one day. The NFC hydrogel was removed from the HCl solution and soaked with water several times until the pH of the rinsing water closes to neutral.

### 2.3. Preparation of NFC-Ag aerogels and NFC aerogels

A freeze-drying method was used to prepare the NFC-Ag and NFC aerogels. The molar amount of $AgNO_3$ added to the NFC dispersion was calculated on the basis of the dried NFC weight. Low quantities were desired to remain below the complete gelation threshold. To 40 g of NFC aqueous dispersion, the calculated amount of $AgNO_3$ corresponding to 0.2 mmol or 0.5 mmol $Ag^+$ per gram of dried NFC (noted as mmol/g in the following text) was dissolved in 1 mL of $H_2O$ and added dropwise under vigorous stirring. After continuously stirring for 30 min, the aqueous dispersion was degassed quickly under vacuum. Eight grams of each sample were put in a glass freeze-drying vial and immersed in an ethanol/dry ice bath. An ethanol/dry ice bath was preferred over liquid $N_2$ for freezing the NFC dispersion as it was found to generate fewer cracks in the aerogel structures. The frozen dispersion was then freeze-dried at a pressure of 0.1 mbar in a FreeZone freeze dry system (Labconco Corporation, USA) without a cooling device for sample containers. The drying was typically finished within 12–24 h. Samples were approximately 5 mm thick with a diameter of 48 mm. To reduce $Ag^+$ to Ag nanoparticles, the dried aerogels were exposed under a UV lamp ($\lambda$ = 320–395 nm) 30 min each for the top side and the bottom side. The same conditions of the freeze-drying process described above were used to prepare the NFC aerogels.

### 2.4. Preparation of NFC-Ag and NFC thin films

NFC films with and without Ag nanoparticles were prepared by ventilated drying. For NFC-Ag films, the calculated amount of $AgNO_3$ in 3 mL of $H_2O$ corresponding to 0.2 mmol $Ag^+$ per gram NFC was added to 50 g of NFC dispersion in a crystallizing dish (100 mm in diameter) under stirring. The mixture was stirred for 30 min, degassed under vacuum, and dried in ventilated oven purged with nitrogen. The $Ag^+$ on the dried film was reduced to Ag nanoparticles through exposure to the UV light for 5 min.

### 2.5. Characterizations

#### 2.5.1. Microscopy

The porous structures of the aerogels were examined using a Hitachi S-4700 field emission scanning electron microscope (FESEM) at an accelerating voltage of 5 kV. The samples were sputter-coated with gold-palladium to reduce charging before SEM operation. Energy-dispersive X-ray spectroscopic (EDX) analysis was performed on the samples without sputter coating, using the

EDX detector connected with FESEM and a voltage of 20 kV. The surface structures of the NFC and NFC-Ag thin films were imaged by an atomic force microscope (AFM) apparatus (Veeco Instruments Inc.) in tapping mode. All scans were performed in air using commercial High-Resolution TappingMode silicon probes with the nominal tip radius of 8 nm. The amplitude setpoint was typically 75% of the free-air oscillation amplitude. The resonance frequency of the cantilever was 310–354 kHz. The NFC nanofibrils and the NFC nanofibrils with Ag nanoparticles were characterized using a JEOL 2100 transmission electron microscope (TEM) operating at 200 kV. The NFC-Ag hydrogel, aerogel or film was dissociated in aqueous solution by stirring overnight followed by centrifuging to get the clear solutions. A short time of sonication was also applied to the hydrogel sample in order to dissociate the nanofibrils. The TEM grid covered with a carbon film was treated with air plasma to increase hydrophilicity of the carbon support film and thus prevent aggregation of the nanofibrils dried on the grid. A droplet of the diluted aqueous dispersion was cast on the grid and remained on the grid for 5 min. Then the extra fluid was removed with the edge of filter paper and the grid was air-dried.

#### 2.5.2. Rheological tests

The dynamic viscoelastic properties of the samples were measured with a rheometer Physica MCR 501 operating in 25 mm parallel-plate configuration and 1 mm gap distance. For the gel samples, 1 mL of NFC dispersion was dispensed to the bottom plate and gelled with 1 mL of metal salt (50 mM) for 10 min before loading the top plate. Stage temperature was maintained at 25 °C and a chamber containing water-saturated tissues was placed around the gels to minimize evaporation. The gel was allowed to sit for 2 h. Frequency sweep experiments were then performed with angular frequency and strain of 0.1–100 rad/s and 0.5%, respectively.

#### 2.5.3. Optical tests

Absorptions of the NFC-Ag hydrogel and the NFC hydrogel were measured from 250 nm to 1000 nm using a Nicolet UV-vis spectrometer. A thin slice (~1 mm) was cut off the hydrogel and put into a quartz cell filled with water. A quartz cell filled with water was used as a blank for taking spectra. The optical properties of the thin films were tested by haze meter Haze-Gard *plus* (BYK-Gardner), which quantifies the visual perception with objective measurement data according to the ASTM standards D 1003 and D 1044. Three specimens were prepared for each sample and measurement for each specimen was repeated three times to get the mean value. Data of transmittance, clarity and haze of the samples were recorded. Transmittance refers to the quantity of incoming light that passes through the sample, clarity refers to the quantity of transmitted light that is scattered at angles less than 2 degrees, and haze refers to the quantity of transmitted light that is scattered at angles greater than 2 degrees.

#### 2.5.4. Specific surface area

The Brunauer–Emmett–Teller (BET) surface areas of samples taken across the top and bottom sides of the aerogels were measured with an Autosorb-1 (Quantachrome Instruments) using $N_2$ gas as the adsorbate for physisorption at 77.4 K. Adsorption/desorption isotherm measurements were collected in the relative pressure range $P/P_0$ from 0.02 to 1. The samples were pretreated in an oven at 100 °C in dry-room for at least 12 h and then outgassed overnight at 105 °C prior to the adsorption analysis. Measurement for each sample was repeated three times.

## 3. Results and discussion

### 3.1. Gelation of NFC with $Ag^+$ and conversion to silver nanoparticles

Fig. 1a shows the "as-produced" NFC aqueous dispersion. Negatively charged carboxylate groups on the TEMPO-oxidized NFC surfaces, neutralized with sodium ions, provide electrostatic repulsion between nanofibrils, preventing them from aggregating while dispersed in water. Although the NFC aqueous dispersion with a concentration of 1.27% exhibits "gel-like" form, it can be easily converted into a low viscosity liquid by vigorous stirring due to the

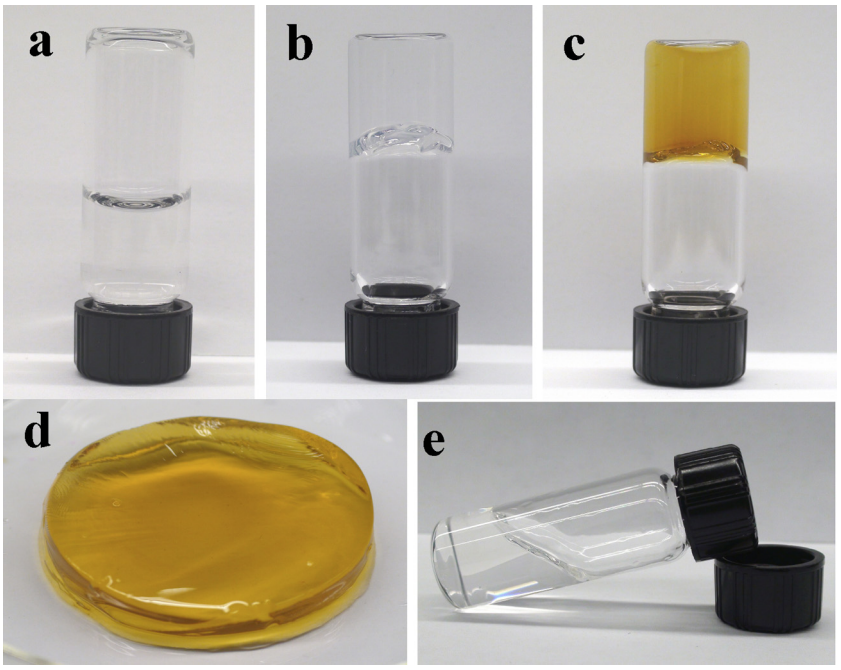


**Fig. 1.** (a) 1.27 wt% NFC in aqueous dispersion, (b) addition of 50 mM $AgNO_3$ to the NFC dispersion initiates gelation of NFC containing $Ag^+$, (c) NFC-$Ag^+$ was slowly reduced to the gel of NFC containing Ag nanoparticles after sitting several days, (d) free-standing NFC-Ag hydrogel, and (e) addition of 50 mM NaCl to the NFC dispersion generates weak gel that can be deformed with shaking.

shear-thinning effect. Addition of 50 mM $AgNO_3$ solution triggered rapid gelation of the NFC, resulting in a strong and colorless gel that could not be deformed by shaking (Fig. 1b). After it sat for five days, a gel with brown color was generated without addition of reducing agent, shown in Fig. 1c. The brown color of the gel indicates the presence of Ag nanoparticles, which were anticipated to form through slow reduction of $Ag^+$ with hydroxyl groups on NFC. Hydroxyl groups are often used as reducing agents in the synthesis of metal nanoparticles. Examples include the synthesis of Au, Ag, Pt, Pd, or Rh nanocrystals through the reduction of noble metal ions by ethanol in the presence of linoleic acid as a stabilizing agent (Wang, Zhuang, Peng, & Li, 2005), and utilizing hyperbranched polyglycidol (Li et al., 2010) as an effective reducing agent for a green protocol to fabricate monometallic and bimetallic nanoparticles. Similarly, the silver ions attached to the nanofibrils should be reduced in situ to the zerovalent metallic state by prevalent hydroxyl groups on the NFC. The gel is strong enough to be picked up and stay in a free-standing form (Fig. 1d). The brown color of gel is visually uniform indicating good distribution of the nanoparticles. The gel has ~4% shrinkage from the volume of NFC aqueous dispersion and contains ~95% water.

It is noteworthy that $Ag^+$ initiated robust gel formation at a substantially lower concentration than that would have been required of $Na^+$. Repeating the same experiment with a comparable $NaNO_3$ solution (50 mM) only yielded a very weak gel that could be deformed by shaking the vial (Fig. 1e). Fig. 2 shows frequency sweep measurement of 1.27% NFC dispersion gelled with 50 mM $AgNO_3$ and 50 mM $NaNO_3$. The value of the storage modulus (G′) for the NFC-$Ag^+$ gel was one order of magnitude higher than the loss modulus (G″), indicating that the gel behaved as an elastic solid. The G′ leveled off at a plateau value of ~6800 Pa and no crossover of G′ and G″ was observed at the studied frequencies. In contrast, G′ of the NFC-$Na^+$ gel was two orders of magnitude lower than that of the NFC-$Ag^+$ gel.

The mechanism for cation-induced gelation of NFC may be derived from analogous behavior described for poly(methacrylic acid) brushes (Konradi & Rühe, 2005). Monovalent alkali metal ions such as $Na^+$ are limited to ionic interactions that, in high quantity, are suggested to provide electrostatic screening of carboxylate groups as well as concentrations of positive charge near the fibril surface. For polymer brushes the resulting changes in polymer chain distances were found to qualitatively agree with theoretical treatments, supporting this description (Konradi & Rühe, 2005). In our study we found similar dependence on concentration such that reducing interfibril repulsion to form stable gels did not occur until

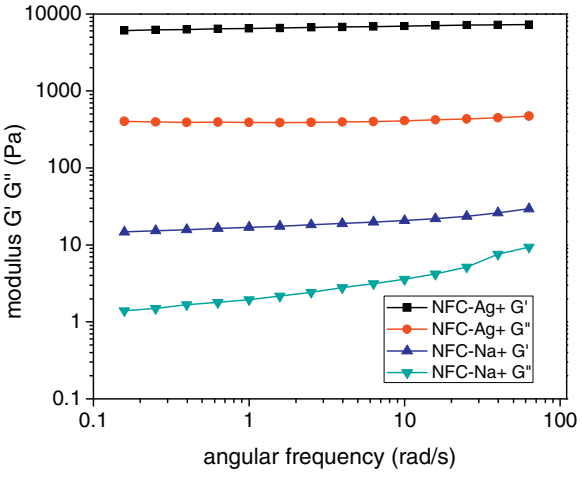


**Fig. 2.** Frequency sweep (0.5% strain) at 25 °C of 1.27% NFC dispersion gelled with 50 mM $AgNO_3$ and 50 mM $NaNO_3$.

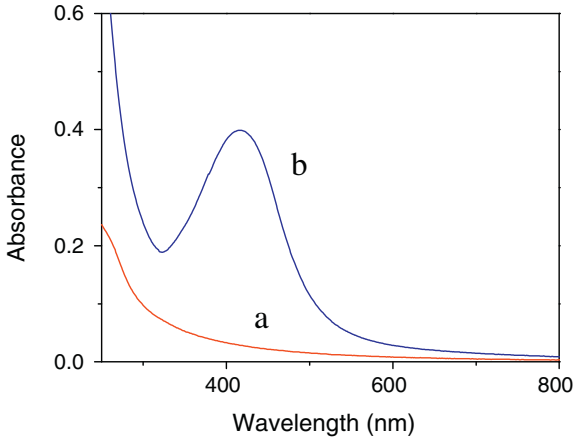


**Fig. 3.** UV–vis spectra of NFC hydrogel (a) and NFC-Ag hydrogel (b). Spectrum of NFC-Ag hydrogel shows characteristic surface plasmon resonance absorption of Ag nanoparticles.

a relatively high number of sodium ions were added. Similar effect was achieved with much smaller number of silver ions because transition metals are capable of additional specific interactions that result in carboxylate metal ion complex formation. Konradi and Rühe found that silver ions caused a dramatic collapse in polymer brush thickness and attributed this result to dehydration as hydrophobic interactions within the polymer metal ion complex outcompeted the solvation power of water (Konradi & Rühe, 2005). We anticipate similar behaviors to be governing gel formation in the current aqueous study. The robust nature of the gel structure is likely the result of widespread hydrogen bonds promoted by the prevalent hydroxyl groups on the fibril surfaces. Preliminary tests in our lab using other metal ions suggest formation of similar gel structures, such as $Ca^{2+}$, $Zn^{2+}$ and $Al^{3+}$. The gelation behaviors of NFC by other metal ions are currently under investigation in our lab.

The spontanous reduction of $Ag^+$ and formation of Ag nanoparticles in the NFC-Ag hydrogel was confirmed by UV–vis spectroscopy and TEM. The optical absorption spectra of an NFC hydrogel and an NFC-Ag hydrogel are shown in Fig. 3. The absorption peak centered at 415 nm for the latter corresponds to the typical surface plasmon resonance (SPR) absorption of metallic silver nanoparticles (Dong, Wang, Sun, & Hinestroza, 2008). NFC dispersions and gels with no silver exhibited minimal UV and visible absorption. Fig. 4 shows the TEM image of Ag nanoparticles on cellulose nanofibrils that were dissociated from the NFC-Ag hydrogel. The presence of nanoparticles is evident in the image, and the average size of the nanoparticles was measured to be 2 nm. The nanofibrils cannot be more clearly revealed without staining, which would mask the presence of Ag, because cellulose usually gives low contrast against carbon support film on the TEM grid.

### 3.2. NFC aerogels with silver nanoparticles

Porous NFC and NFC-Ag aerogels were dried by direct water removal from the dispersions using the freeze-drying method. Fig. 5a shows a typical NFC aerogel, with a thickness of about 5 mm, prepared from 1.27 wt% NFC aqueous dispersion. The porous structure of the aerogel was investigated by FESEM with representative micrographs presented in Fig. 6a and b. The aerogel consisted of an open network of extended sheet-like structures forming macroscopic channels, in which the thin sheets comprised aggregated nanofibrils as revealed in the high magnification FESEM images. Asymmetric porosity was observed for the top layer that faced to the air during drying and the bottom layer that was in contact with

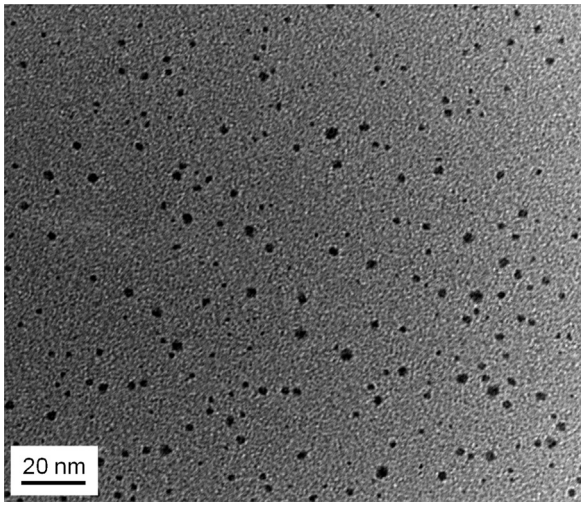


**Fig. 4.** Transmission electron micrograph of Ag nanoparticles on NFC dissociated from NFC-Ag hydrogel. The image shows the nanoparticles only, since the nanofibrillated cellulose gives very low contrast against the carbon support film on TEM grid without staining.

the vial immersed in the freezing bath. The top layer of the aerogel (Fig. 6a) had large open pores ranging from tens to hundreds of micrometers in diameter with nanofibril bundles protruding from the surface of the sheet. The bottom layer (Fig. 6b) had finer pores and a mixture of three dimensional open networks of nanofibrils and cell wall sheet structures, owing to the faster cooling than the top layer while freezing. In the vertical surface direction the NFC aerogel had a lamellar structure. The BET surface area measured using an $N_2$ adsorption–desorption method was calculated to be 20 $m^2/g$, which is in similar range as that of freeze-dried NFC aerogels with nanofibrils having been pretreated with carboxymethylation (Sehaqui, Salajkov, et al., 2010). Different drying methods, such as supercrital-$CO_2$ drying and freeze drying from *tert*-butyl alcohol as a solvent, could result in much higher BET surface area of several hundreds of $m^2/g$ due to less aggregation of the nanofibrils in the aerogel (Korhonen et al., 2011; Saito et al., 2011).

Fig. 5b and c shows photographs of the NFC-Ag aerogels obtained from the samples with 0.2 mmol/g and 0.5 mmol/g $AgNO_3$, respectively, after freeze-drying and reduction. Introduction of Ag species caused a color change from white to brown characteristic for Ag nanoparticles. The NFC-Ag aerogel obtained from 0.2 mmol/g $AgNO_3$ has deeper color in the middle than the edge attributed to variance in the pore size and subsequent UV reduction non-uniformity. The variance in pore size may be caused by differences in cooling rates that result in larger crystal ice developing in the middle than at the edge.

Fig. 6c–f includes FESEM images of the NFC-Ag aerogels, which demonstrated open networks of extended sheet-like structures similar to the NFC aerogel. Comparison of Fig. 6a, c and e indicates that these structures were accompanied by closure of the surface texture with increasing silver concentration. The aerogel derived from 0.2 mmol/g $AgNO_3$ has similar surface texture as that of the neat NFC aerogel except a few cell closures. The aerogel derived from 0.5 mmol/g $AgNO_3$ had a more closed surface texture than the NFC aerogel. The bottom layers of NFC-Ag aerogels shown in Fig. 6d and f have pore structures and open networks of nanofibrils, similar to that of pure NFC aerogel. The changing top surface texture is reflected in reduced surface areas. The NFC aerogels obtained using no silver, 0.2 mmol/g Ag and 0.5 mmol/g Ag had respective BET specific surface areas of 20 $m^2/g$, 15 $m^2/g$, and 8 $m^2/g$.

Fig. 7 presents the TEM images of Ag-treated cellulose nanofibrils that were dissociated from the NFC-Ag aerogels. The presence of spherical nanoparticles is clearly revealed in both images. The average sizes of the nanoparticles were measured to be 3 nm and 4 nm for the aerogels prepared from $AgNO_3$ 0.2 mmol/g and 0.5 mmol/g, respectively. The nanofibrils are faintly evident along the arrays of nanoparticles in the images. The nanofibrils cannot be more clearly revealed without staining because of the low image contrast of cellulose against carbon support film on the TEM grid. EDX spectra in Fig. 8, which were collected from the samples imaged by FESEM, show the presence of Ag signal peaks, indicating the nanoparticles are silver. The brown color of NFC-Ag aerogels also suggests the presence of Ag nanoparticles in the aerogels. The sodium peaks in the EDX spectra come from the sodium ions that were used to neutralize carboxylate groups in the "as-produced" NFC dispersion.

### 3.3. NFC films decorated with silver nanoparticles

An 80 μm NFC thin film was prepared directly from the as-received NFC aqueous dispersion by solution-casting (Fig. 9a). The introduction of silver to the NFC thin film using 0.2 mmol/g $AgNO_3$ yielded a uniform brown color of Ag nanoparticles after reduction (Fig. 9b), which was attributed to the surface plasmon resonance absorption of well-distributed Ag nanoparticles. The incorporation of the nanoparticles does not impact integrity of the film. The formation of nanoparticles and the composition were confirmed by TEM and EDX analyses, shown in Figs. 2S and 3S (supplementary information). Most of the nanoparticles have fairly small sizes with an average of 2 nm owing to the short UV reduction time (5 min) applied to the film.

The NFC film was highly transparent. The UV–vis transmittance at 550 nm was 89% for the 80 μm NFC film. The extensive absorption band of Ag nanoparticles in the visible range interfered with UV–vis spectroscopy on the NFC-Ag film. Additional optical studies were carried out with a haze meter to investigate scattering behavior of both NFC and NFC-Ag films, listed in Table 1. The high transmittance, low haze and high clarity of NFC films are typical for well formed thin films of these materials. The substantial decrease in transmittance with incorporation of Ag nanoparticles is due to the strong absorption of Ag nanoparticles, however the NFC-Ag film maintains high clarity and low haze indicating low aggregation of Ag nanoparticles. The slight increase in haze may be caused by scattering via the Ag nanoparticles.

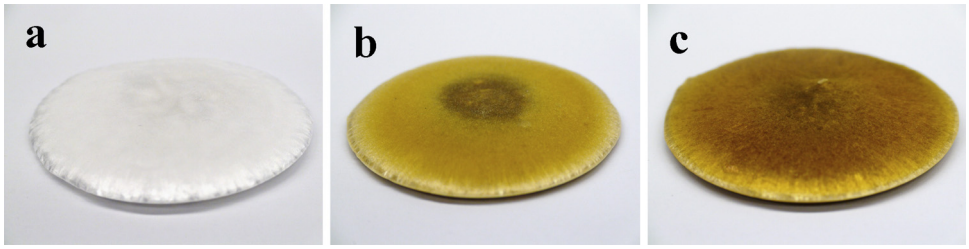


**Fig. 5.** (a) NFC aerogel, (b) NFC aerogel with Ag nanoparticles obtained from 0.2 mmol/g $AgNO_3$, and (c) NFC aerogel with Ag nanoparticles obtained from 0.5 mmol/g $AgNO_3$. All the aerogels were prepared by freeze-drying process.

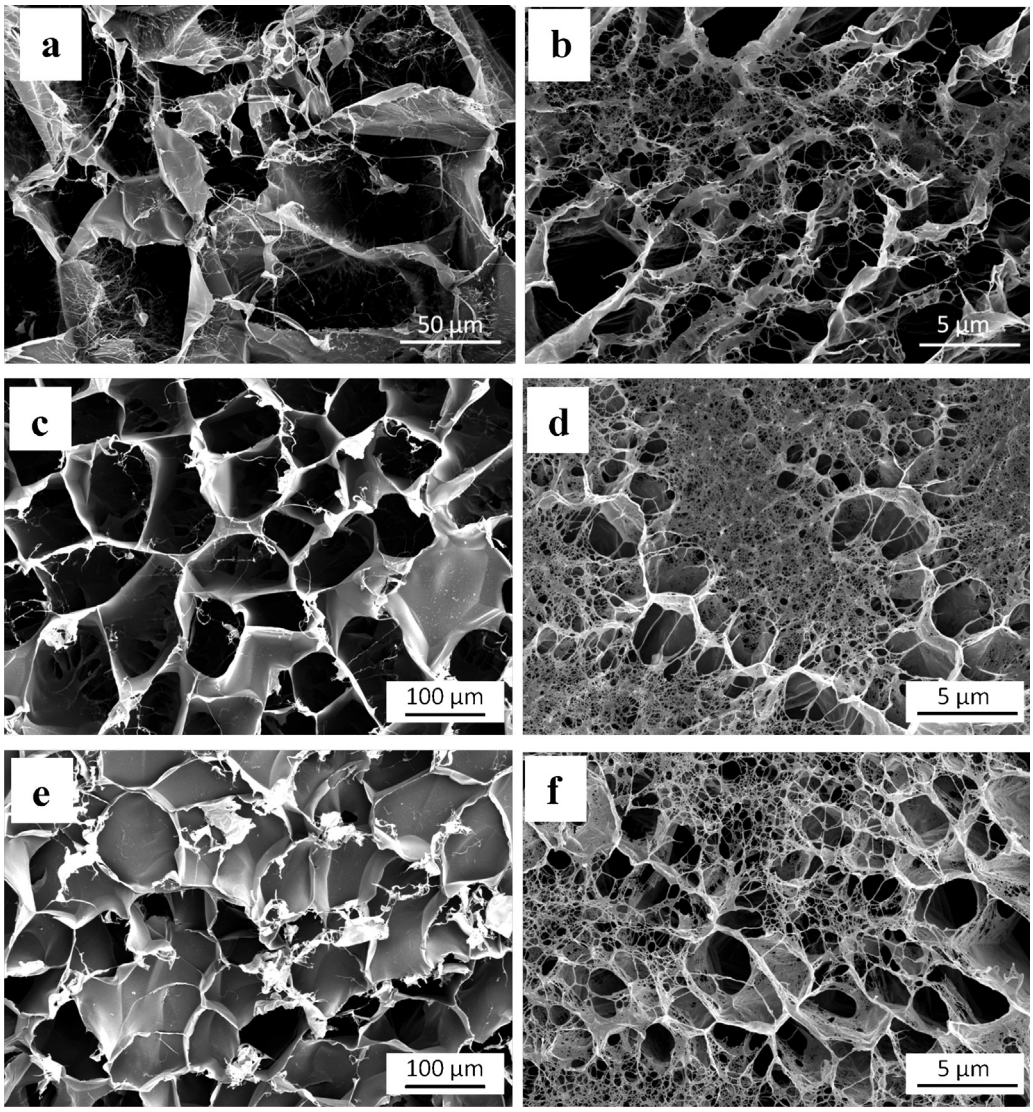


**Fig. 6.** FESEM micrographs of the freeze-dried aerogel structures: NFC aerogel (a–b), and NFC aerogels decorated with Ag nanoparticles generated from (c–d) 0.2 mmol/g $AgNO_3$ and (e–f) 0.5 mmol/g $AgNO_3$. (a), (c) and (e) Top surfaces of the aerogels. (b), (d) and (f) Bottom surfaces of the aerogels.

Fig. 10 shows AFM phase images characterizing surface morphologies of the NFC film and the NFC-Ag film. The AFM scans of the NFC film and the NFC-Ag film were carried out using the same type of probes for the purpose of comparison. In Fig. 10a, the nanofibrils entangle and form a fibrous network matrix consisting of randomly assembled nanofibrils. The film has a macroscopically smooth surface with surface roughness RMS (root mean square) 4 nm via analyzing the topography scans of the film's surface. The

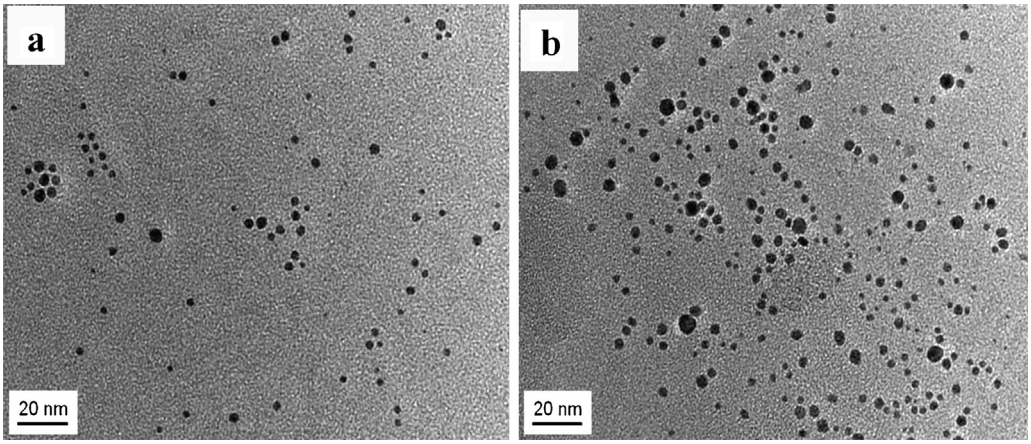


**Fig. 7.** Transmission electron micrographs of NFC with Ag nanoparticles obtained from 0.2 mmol/g $AgNO_3$ (a) and 0.5 mmol/g $AgNO_3$ (b). The image shows the nanoparticles only, since the nanofibrillated cellulose gives very low contrast against the carbon support film on TEM grid without staining.

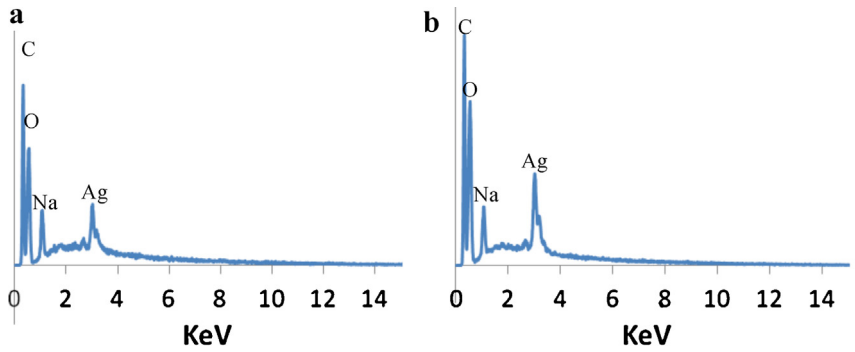


**Fig. 8.** Energy-dispersive X-ray spectra collected from (a) NFC-Ag aerogel (0.2 mmol/g $AgNO_3$) and (b) NFC-Ag aerogel (0.5 mmol/g $AgNO_3$).

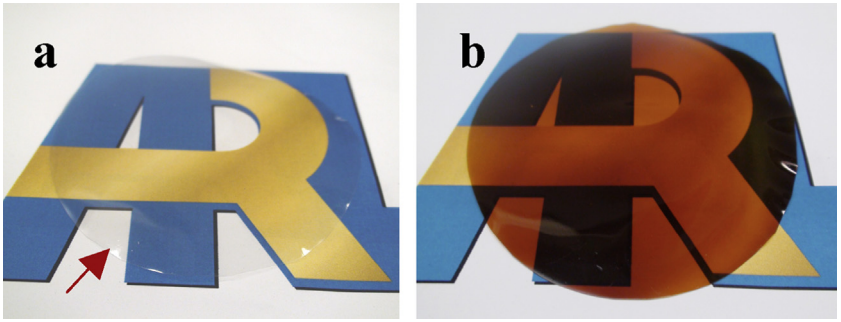


**Fig. 9.** Photos of (a) NFC transparent film and (b) NFC film decorated with Ag nanoparticles. Both films have thickness of 80 μm.

**Table 1**
Optical properties obtained from a haze meter for 80 μm thick NFC and NFC-Ag films.

| Sample | Transmittance (%) | Haze (%) | Clarity (%) |
|---|---|---|---|
| NFC film | 91.3 | 1.08 | 99.5 |
| NFC-Ag film | 23.4 | 2.24 | 97.8 |

NFC-Ag film (Fig. 10b) has a similar entangled fibrous network surface morphology as the NFC film. The surface roughness RMS of NFC-Ag film was measured to be 2 nm, lower than that of the NFC film. The Ag nanoparticles could not be clearly resolved due to the small size. Interestingly, the Ag-modified nanofibrils exhibited consistently smaller diameters than those in the NFC film from the repeated scans, which were estimated from AFM height images to be 8 nm and 14 nm, respectively. A close examination of the NFC surface by enlarging the image or scanning at a smaller area showed coalescence of nanofibrils to give wider fibers. The coalescence of NFCs likely forms as a result of prevalent hydrogen bonding interactions, possibly mediated by water molecules, that bridge adjacent nanofibrils during drying. It seems likely that the strong binding of carboxylate groups on the nanofibrils with Ag species limits its solvation with water in aqueous dispersion and subsequent hydrogen bonding with groups on adjacent nanofibrils after water removal, and thus decreases coalescence of nanofibrils. This is consistent with previous studies on poly(methacrylic acid) brushes where the

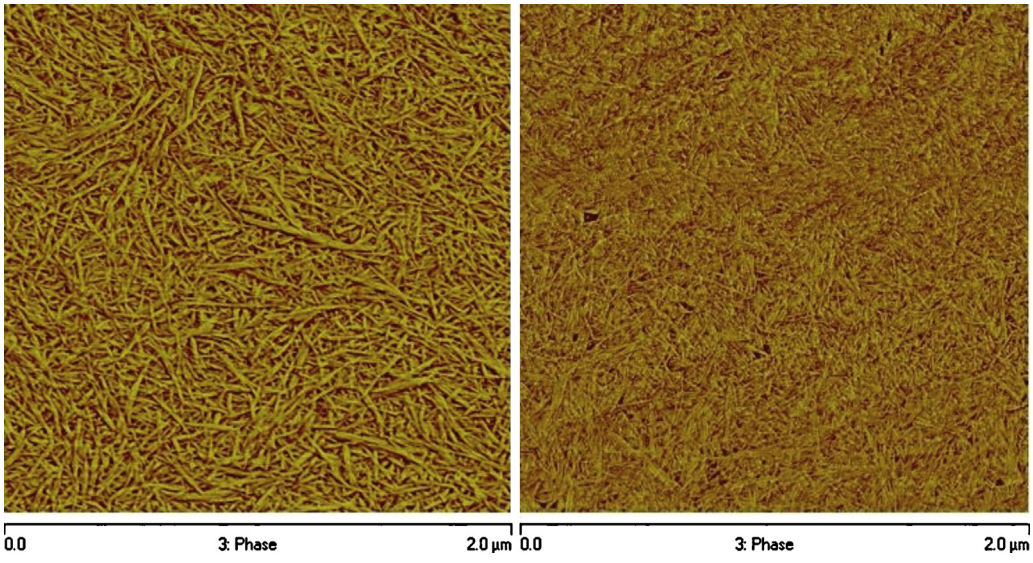


**Fig. 10.** AFM phase images of (a) film surface of NFC and (b) film surface of NFC-Ag.

brushes become more hydrophobic with increasing silver ion loading due to charge recombination and concurrent dehydration as a result of specific binding (Konradi & Rühe, 2005).

The importance of these materials is based on their potential biocompatibility and degradability as well as the potential low cost and ready availability of nature-derived nanocellulose. The addition of metal nanoparticles adds new functionalities such that these structured materials may be of interest in diverse applications such as electronics, sensors, wound dressings, catalysis, and selective filtration. For example, we performed preliminary testing of the antimicrobial ability of NFC-Ag hydrogel as a potential wound dressing material to inhibit the growth of Escherichia coli (Gram-negative) and Staphylococcus aureus (Gram-positive) using Kirby Bauer protocol. The NFC-Ag hydrogel was effective against both gram negative and gram positive bacteria whereas the NFC hydrogel as control exhibited no inhibition to the bacteria growth (see supplementary information Fig. 4S).

## 4. Conclusion

We have prepared network structured materials of NFC functionalized with silver nanoparticles and revealed the gelation effect of silver salt on the NFC aqueous dispersion. The gelation of the TEMPO-oxidized NFC aqueous dispersion was triggered by strong association of carboxylate groups on NFC with $Ag^+$, yielding a self-supporting functionalized hydrogel. The stiff NFC-$Ag^+$ gel had a storage modulus of ~6800 Pa, two orders of magnitude higher than that of NFC with comparable amount of $Na^+$. The addition of a low amount of Ag species reduced coalescence of nanofibrils in the smooth NFC-Ag film.

Using silver as an example, we have demonstrated the ease with which coordination compounds and nanoparticles of transition metals may be applied to structured nanocellulose. We expect that these techniques can be translated to other metal ions with similar ease. A greater range of structures and properties are also suggested in future studies by exploring transition and alkali earth metals capable of effectively reducing surface charges or bridging two or more surface groups on the cellulose nanofibril to enact more highly reinforced network structures.

## Acknowledgements

This research was supported in part by an appointment to the Postgraduate Research Participation Program at the U.S. Army Research Laboratory administered by the Oak Ridge Institute for Science and Education through an interagency agreement between the U.S. Department of Energy and USARL. The authors thank Dr. Alan Rudie and Mr. Richard Reiner in USDA Forest Product Laboratory for supplying the nanocellulose dispersion, as well as Dr. Lars Piehler, Dr. Josh Orlicki and Dr. Kenneth Strawhecker at USARL for many useful discussions.

## Appendix A. Supplementary data

Supplementary data associated with this article can be found, in the online version, at http://dx.doi.org/10.1016/j.carbpol.2013.03.041.

## References

Aulin, C., Netrval, J., Wågberg, L., & Lindström, T. (2010). Aerogels from nanofibrillated cellulose with tunable oleophobicity. *Soft Matter*, *6*(14), 3298–3305.

Chang, C. Y., & Zhang, L. N. (2011). Cellulose-based hydrogels: Present status and application prospects. *Carbohydrate Polymers*, *84*(1), 40–53.

Diez, I., Eronen, P., Osterberg, M., Linder, M. B., Ikkala, O., & Ras, R. H. A. (2011). Functionalization of nanofibrillated cellulose with silver nanoclusters: Fluorescence and antibacterial activity. *Macromolecular Bioscience*, *11*(9), 1185–1191.

Dong, H., Strawhecker, K. E., Snyder, J. F., Orlicki, J. A., Reiner, R. S., & Rudie, A. W. (2012). Cellulose nanocrystals as a reinforcing material for electrospun poly(methyl methacrylate) fibers: Formation, properties and nanomechanical characterization. *Carbohydrate Polymers*, *87*(4), 2488–2495.

Dong, H., Wang, D., Sun, G., & Hinestroza, J. P. (2008). Assembly of metal nanoparticles on electrospun nylon 6 nanofibers by control of interfacial hydrogen-bonding interactions. *Chemistry of Materials*, *20*(21), 6627–6632.

Eichhorn, S. J., Dufresne, A., Aranguren, M., Marcovich, N. E., Capadona, J. R., Rowan, S. J., et al. (2010). Review: Current international research into cellulose nanofibres and nanocomposites. *Journal of Materials Science*, *45*(1), 1–33.

Fall, A. B., Lindström, S. B., Sundman, O., Ödberg, L., & Wågberg, L. (2011). Colloidal stability of aqueous nanofibrillated cellulose dispersions. *Langmuir*, *27*(18), 11332–11338.

Fukuzumi, H., Saito, T., Iwata, T., Kumamoto, Y., & Isogai, A. (2009). Transparent and high gas barrier films of cellulose nanofibers prepared by TEMPO-mediated oxidation. *Biomacromolecules*, *10*(1), 162–165.

Garcia-Gonzalez, C. A., Alnaief, M., & Smirnova, I. (2011). Polysaccharide-based aerogels – Promising biodegradable carriers for drug delivery systems. *Carbohydrate Polymers*, *86*(4), 1425–1438.

Henriksson, M., Berglund, L. A., Isaksson, P., Lindström, T., & Nishino, T. (2008). Cellulose nanopaper structures of high toughness. *Biomacromolecules*, *9*(6), 1579–1585.

Ifuku, S., Tsuji, M., Morimoto, M., Saimoto, H., & Yano, H. (2009). Synthesis of silver nanoparticles templated by TEMPO-mediated oxidized bacterial cellulose nanofibers. *Biomacromolecules*, *10*(9), 2714–2717.

Jin, H., Nishiyama, Y., Wada, M., & Kuga, S. (2004). Nanofibrillar cellulose aerogels. *Colloids and Surfaces A – Physicochemical and Engineering*, *240*(1-3), 63–67.

Koga, H., Tokunaga, E., Hidaka, M., Umemura, Y., Saito, T., Isogai, A., et al. (2010). Topochemical synthesis and catalysis of metal nanoparticles exposed on crystalline cellulose nanofibers. *Chemical Communications*, *46*(45), 8567–8569.

Konradi, R., & Rühe, J. (2005). Interaction of poly(methacrylic acid) brushes with metal ions: Swelling properties. *Macromolecules*, *38*(10), 4345–4354.

Korhonen, J. T., Hiekkataipale, P., Malm, J., Karppinen, M., Ikkala, O., & Ras, R. H. A. (2011). Inorganic hollow nanotube aerogels by atomic layer deposition onto native nanocellulose templates. *ACS Nano*, *5*(3), 1967–1974.

Li, H., Jo, J. K., Zhang, L. D., Ha, C. S., Suh, H., & Kim, I. (2010). Hyperbranched polyglycidol assisted green synthetic protocols for the preparation of multifunctional metal nanoparticles. *Langmuir*, *26*(23), 18442–18453.

Liu, H., Wang, D., Song, Z. Q., & Shang, S. B. (2011). Preparation of silver nanoparticles on cellulose nanocrystals and the application in electrochemical detection of DNA hybridization. *Cellulose*, *18*(1), 67–74.

Mahmoud, K. A., Male, K. B., Hrapovic, S., & Luong, J. H. T. (2009). Cellulose nanocrystal/gold nanoparticle composite as a matrix for enzyme immobilization. *ACS Applied Materials and Interfaces*, *1*(7), 1383–1386.

Moon, R. J., Martini, A., Nairn, J., Simonsen, J., & Youngblood, J. (2011). Cellulose nanomaterials review: Structure, properties and nanocomposites. *Chemical Society Reviews*, *40*(7), 3941–3994.

Pääkkö, M., Vapaavuori, J., Silvennoinen, R., Kosonen, H., Ankerfors, M., Lindström, T., et al. (2008). Long and entangled native cellulose I nanofibers allow flexible aerogels and hierarchically porous templates for functionalities. *Soft Matter*, *4*(12), 2492–2499.

Padalkar, S., Capadona, J. R., Rowan, S. J., Weder, C., Won, Y.-H., Stanciu, L. A., et al. (2010). Natural biopolymers: Novel templates for the synthesis of nanostructures. *Langmuir*, *26*(11), 8497–8502.

Saito, T., & Isogai, A. (2005). Ion-exchange behavior of carboxylate groups in fibrous cellulose oxidized by the TEMPO-mediated system. *Carbohydrate Polymers*, *61*(2), 183–190.

Saito, T., Kimura, S., Nishiyama, Y., & Isogai, A. (2007). Cellulose nanofibers prepared by TEMPO-mediated oxidation of native cellulose. *Biomacromolecules*, *8*(8), 2485–2491.

Saito, T., Uematsu, T., Kimura, S., Enomae, T., & Isogai, A. (2011). Self-aligned integration of native cellulose nanofibrils towards producing diverse bulk materials. *Soft Matter*, *7*(19), 8804–8809.

Sehaqui, H., Salajkov, M., Zhou, Q., & Berglund, L. A. (2010). Mechanical performance tailoring of tough ultra-high porosity foams prepared from cellulose I nanofiber suspensions. *Soft Matter*, *6*(8), 1824–1832.

Sehaqui, H., Liu, A. D., Zhou, Q., & Berglund, L. A. (2010). Fast preparation procedure for large, flat cellulose and cellulose/inorganic nanopaper structures. *Biomacromolecules*, *11*(9), 2195–2198.

Shin, Y., Bae, I.-T., Arey, B. W., & Exarhos, G. J. (2008). Facile stabilization of gold-silver alloy nanoparticles on cellulose nanocrystal. *Journal of Physical Chemistry C*, *112*(13), 4844–4848.

Wang, X., Zhuang, J., Peng, Q., & Li, Y. (2005). A general strategy for nanocrystal synthesis. *Nature*, *437*(7055), 121–124.

Wu, M., Kuga, S., & Huang, Y. (2008). Quasi-one-dimensional arrangement of silver nanoparticles templated by cellulose microfibrils. *Langmuir*, *24*(18), 10494–10497.